Size-Dependent Reaction Cross Section of Protonated Water Clusters $H^+(H_2O)_n$ ($n = 2-11$) with D_2O

Satoru Yamaguchi,[†,‡,#] Satoshi Kudoh,[‡,⊥] Yoshiki Okada,*[,‡] Takaaki Orii,[‡,∥] Kazuo Takeuchi,[†,‡] Takashi Ichikawa,[§] and Hiromi Nakai[§]

Graduate School of Science and Engineering, Saitama University, 255, Shimoohkubo, Saitama-shi, Saitama 338-8570, Japan, RIKEN (The Institute of Physical and Chemical Research), 2-1 Hirosawa, Wako-shi, Saitama 351-0198, Japan, and Department of Chemistry, School of Science and Engineering, Waseda University, Tokyo 169-8555, Japan

Received: January 17, 2003; In Final Form: October 17, 2003

Collisional dynamics of size- and translational-energy-selected protonated water clusters $H^+(H_2O)_n$ ($n = 2-11$) in single collisions with D_2O were investigated using guided-ion beam tandem mass spectrometry. The dominant reaction channel for the collision involves the incorporation of D_2O into $H^+(H_2O)_n$ at low collision energy, whereas at high collision energy, the dissociation of $H^+(H_2O)_n$ is predominant. The measured total reaction cross section of $H^+(H_2O)_n$ with D_2O is found to depend strongly on the cluster size; the cross section drastically increases as the cluster size increases from $n = 4$ to 5, 6 to 7, and 8 to 9 and has local minima at $n = 6$ and 8 at collision energies of 0.05 and 0.10 eV, respectively. The size dependence of the total cross section is discussed herein in terms of a comparison with the collision cross section obtained from ab initio calculations.

Introduction

Protonated water clusters $H^+(H_2O)_n$ are abundant in the earth's atmosphere. $H^+(H_2O)_n$ is important in ion chemistry in the lower ionosphere and stratosphere.[1] In addition, $H^+(H_2O)_n$ in the troposphere plays an important role as a generation source of aerosol particles.[2] Studies of the properties of $H^+(H_2O)_n$ clusters, including their structures and chemical dynamics, are essential to a further understanding of cluster science, with particular attention being paid to their size-specific properties.[3] For instance, the structures of $H^+(H_2O)_n$ have been studied theoretically, and it is known that two candidates for the ion core of $H^+(H_2O)_n$ are the H_3O^+ and $H_5O_2^+$ cations, called the Eigen cation[4] and the Zundel cation,[5] respectively. The nature of the exact form of $H^+(H_2O)_n$ has been discussed extensively.[6−11] Recently, measurements of vibrational predissociation spectroscopy and ab initio calculations have indicated that $H^+(H_2O)_3$ and $H^+(H_2O)_4$ possess the Eigen cation, whereas $H^+(H_2O)_6$ is a mixture of isomers with the Eigen and Zundel cations, respectively, and that the energy difference between these two isomers is insignificant.[12]

The reactions of $H^+(H_2O)_n$ with a variety of atmospheric molecules have been studied. The reaction mechanism (e.g., proton and ligand transfer from the cluster to reactants, ligand switching between the cluster and reactants, and the association of the reactant with the cluster) and its rate have been investigated experimentally.[13,14] For instance, the reactions of $H^+(H_2O)_n$ with chlorine nitrate $ClONO_2$, an important "reservoir compound" involved in the stratospheric ozone chemistry, were investigated in order to study the role of heterogeneously catalyzed reactions in ozone depletion.[15] It was found in that study that hypochlorous acid HOCl, a molecule related to ozone destruction, is produced by hydrolysis on the $H^+(H_2O)_n$ cluster surface and evaporates almost immediately from the cluster.

The bimolecular reactions of $H^+(H_2O)_n$ ($n = 2-4$) with D_2O were studied using a selected ion-flow tube apparatus.[16] It was revealed that thorough randomization of the H and D atoms occurs prior to unimolecular dissociation in the ion−molecule transient complex. However, this kind of study has typically been undertaken under multiple-collision conditions, which introduce undesired complexity to our understanding of the reaction mechanism. In addition, the collisional dynamics of $H^+(H_2O)_n$, which are related to the size and structure of the cluster, have not yet been satisfactorily elucidated, despite the size dependence of chemical and physical properties being one of the important issues of atmospheric chemistry and cluster science.

In the present study, we investigated the collisions of size- and translational-energy-selected $H^+(H_2O)_n$ ($n = 2-11$) under single-collision conditions with D_2O using guided-ion beam tandem mass spectrometry to clarify the size-specific collisional dynamics of $H^+(H_2O)_n$.

Experimental Section

Figure 1 shows a schematic drawing of the apparatus employed in this experiment. A detailed description of the

* To whom correspondence should be addressed. Fax: +81-462-4702. E-mail: yokada@riken.jp.
† Saitama University.
‡ RIKEN.
§ Waseda University.
⊥ Present address: Graduate School of Bio-Applications and Systems Engineering (BASE), Tokyo University of Agriculture and Technology, 3-5-8 Saiwai-cho, Koganei-shi, Tokyo 183-8509, Japan.
∥ Present address:Research Center for Advanced Manufacturing on Nanoscale Science and Engineering, National Institute of Advanced Industrial Science and Technology (AIST), 1-2-1 Namiki, Tsukuba, Ibaraki 305-8564, Japan.
Present address: Power and Industrial Systems R&D Laboratory, Hitachi, Ltd., 832-2, Horiguchi, Hitachinaka-shi, Ibaraki 312-0034, Japan.

10.1021/jp034129h CCC: $25.00
Published on Web 11/22/2003

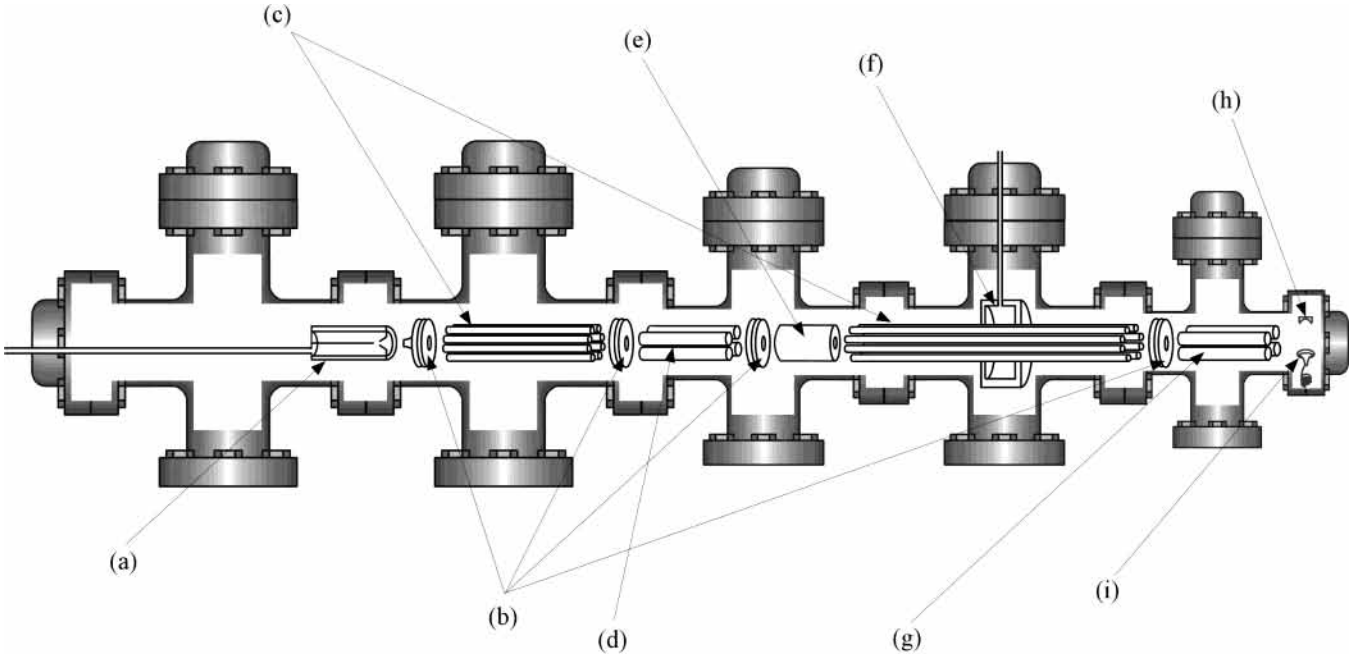

Figure 1. Schematic diagram of the apparatus: (a) corona discharge cluster ion source; (b) ion optics; (c) octopole ion beam guide; (d) quadrupole mass filter; (e) Bessel box energy analyzer; (f) collision cell; (g) quadropole mass analyzer; (h) ion-conversion dynode; (i) secondary electron multiplier.

apparatus and experimental procedures are given elsewhere.[17] Thus, only the details pertinent to this experiment are given here. Nitrogen gas bubbled through a water reservoir at 25 °C was introduced to the corona discharge cluster ion source, and protonated water clusters $H^+(H_2O)_n$ ($n = 2-11$) were produced in a free jet through a nozzle 100 μm in diameter. The cluster ions were focused by a series of ion optics and transferred by the first octopole ion beam guide (OPIG) into a quadrupole mass filter. The size-selected cluster ions passing through the mass filter were focused by a series of ion optics into a Bessel box translational energy analyzer. The translational energy distributions of the size-selected cluster ions were narrowed to approximately 0.03 eV in the center-of-mass frame by the Bessel box translational energy analyzer. The size-selected and translational-energy-selected cluster ions were focused by a series of ion optics into a collision cell equipped with the second OPIG. The collision cell was filled with D_2O gas at pressures of $5-6 \times 10^{-6}$ Torr, where $H^+(H_2O)_n$ was allowed to collide with a D_2O molecule. It was confirmed that the single-collision conditions were fulfilled in the given pressure range because no fragments of multiple-collision product ions were observed. After the collision cell, the cluster ions were focused by ion optics into a quadropole mass spectrometer to be mass-analyzed. The mass-selected ions were detected by a secondary electron multiplier equipped with an ion-conversion dynode. The pressure of the collision cell was monitored with a spinning rotor gauge. The background pressure in the collision cell was less than 2×10^{-7} Torr. The temperature of D_2O gas in the collision cell was 25 °C. The collision energies were controlled by changing the DC potential of the second OPIG. We measured the translational energy distribution of the parent cluster ions and determined the collision energy at the center of the distribution.

Results

Figure 2a−c shows typical mass spectra of the cluster ions produced from $H^+(H_2O)_3$ with and without the target gas D_2O in the collision cell, respectively. The cluster ions observed were the parent ion $H^+(H_2O)_3$ at 55 *m*/*z* and the daughter ion $H^+(H_2O)_2$ at 37 *m*/*z* without the target gas, as shown in Figure 2c. With the target gas D_2O in the collision cell, the ions observed were $H^+(H_2O)_2(D_2O)$ at 57 *m*/*z*, $H^+(H_2O)_2(HDO)$ at 56 *m*/*z*, $H^+(H_2O)_3$ at 55 *m*/*z*, $H^+(H_2O)(D_2O)$ at 39 *m*/*z*, $H^+(H_2O)(HDO)$ at 38 *m*/*z*, and $H^+(H_2O)_2$ at 37 *m*/*z*, as shown in Figure 2, parts a and b. We observed the ions containing D_2O at 57 and 39 *m*/*z* and ions produced by the H/D exchange reaction at 56 and 38 *m*/*z* in the collision of $H^+(H_2O)_3$ with D_2O. When the collision energy was 1.00 eV, as shown in Figure 2a, these ions drastically decreased compared with those in Figure 2b at the collision energy of 0.10 eV. The products that contained D_2O and HDO molecules and those that did not contain D atoms were also observed for other sizes of protonated water clusters $H^+(H_2O)_n$ ($n = 2-11$). The overlapping mass spectra peaks in Figure 2 were deconvoluted by fitting them

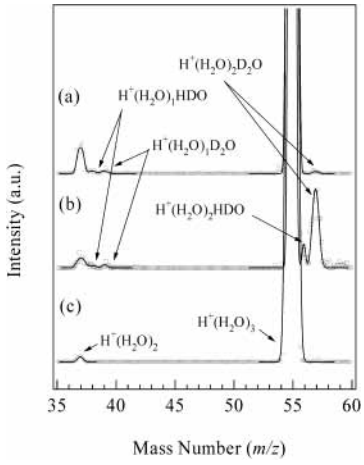

Figure 2. Typical mass spectra of the cluster ions produced from $H^+(H_2O)_3$ with the target gas D_2O in the collision cell: (a) at a collision energy of 1.00 eV in the center-of-mass frame and (b) at a collision energy of 0.10 eV. (c) The mass spectra of the cluster ions produced from $H^+(H_2O)_3$ without the target gas D_2O in the collision cell.

SCHEME 1

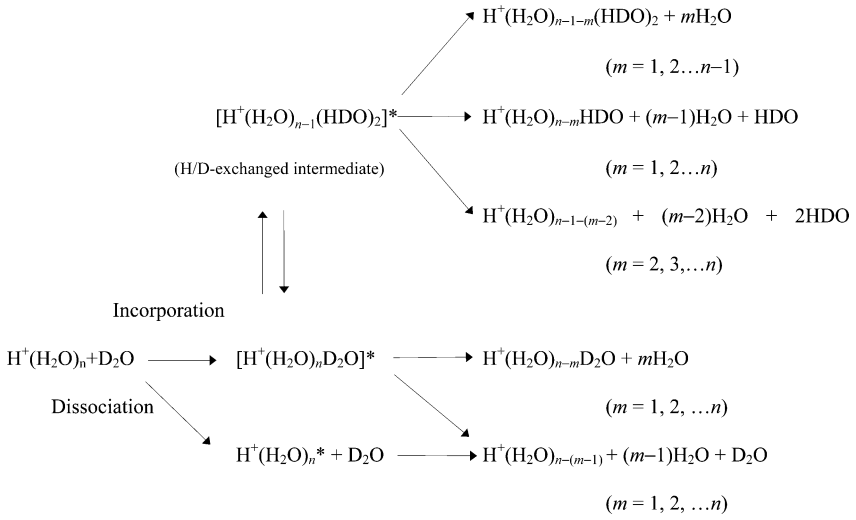

with modified Gaussian functions. The intensities of these peaks were calculated from the integrated area of the modified Gaussians curves.

Discussion

1. Reaction Scheme. In addition to the parent cluster ion, three types of product cluster ions, including the H/D-unexchanged incorporation product containing a D_2O molecule, the H/D-exchanged incorporation product containing HDO molecules, and the dissociation product containing no D atoms, were observed in the collision of $H^+(H_2O)_n$ ($n = 2-11$) with a D_2O molecule, as shown in Figure 2, parts a and b. The reaction mechanism is considered to be as follows.[18] In the incorporation process, the D_2O molecule is first captured by the parent cluster ion to form a hot cluster ion, $H^+(H_2O)_nD_2O^*$. The H/D-exchanged intermediate, $H^+(H_2O)_{n-1}(HDO)_2^*$, is then generated by a randomization of H and D atoms. Subsequently, several H_2O and HDO molecules and one D_2O molecule are released from either of the hot ions. In the dissociation process, the parent cluster ion is heated by collision energy transfer from the D_2O molecule and subsequently releases some H_2O molecules. All of the reaction pathways are described in Scheme 1.

A similar reaction scheme has been proposed in the cases of collision-induced reactions of $H^+(NH_3)_n$ with ND_3 and Ar_n^+ with ^{36}Ar,[17,19] though no proof of a H/D exchange reaction was seen in the former case.

2. Reaction Cross Section. The total cross section σ_n^r was calculated as

$$\sigma_n^r = \frac{k_B T}{Pl} \ln \frac{I_n^0}{I_n^l} \tag{1}$$

where I_n^0 and I_n^l are the intensities of the parent cluster ions at the entrance and exit of the collision cell, respectively, l is the effective path length of the collision cell, P and T are the pressure and temperature of the target gas, respectively, and k_B is the Boltzmann constant. The daughter ions $H^+(H_2O)_n$ ($n < 3$) were observed even without the target gas, as shown in Figure 2c. These ions were produced by unimolecular dissociation of the parent cluster ion. The daughter cluster ions produced by unimolecular dissociation were included in the mass spectra obtained with the target gas. Therefore, the values of I_n^0 and I_n^l can be evaluated by the following equations, in the same manner as that reported in ref 17:

$$I_n^0 = (i_n^P + \sum_{m=1}^{n} i_{n-m}^{Uex} + \sum_{m=1}^{n} i_{n-m}^{Ex} + \sum_{m=1}^{n} i_{n-m}^{D}) S_n^n \tag{2}$$

$$I_n^l = i_n^P \tag{3}$$

and

$$S_n^{n-m} = \frac{i_{n-m}^U}{\sum_{m=0}^{n-1} i_{n-m}^U} \tag{4}$$

where i_n^P, i_{n-m}^{Uex}, i_{n-m}^{Ex}, i_{n-m}^D, and i_{n-m}^U represent the intensities of the parent cluster ions, the cluster ions produced by the loss of m ($m = 1, 2, 3, \ldots, n$) molecules of H_2O from $H^+(H_2O)_n(D_2O)^*$, those produced by the loss of $m - 1$ ($m = 1, 2, 3, \ldots, n$) molecules of H_2O and one molecule of HDO from $H^+(H_2O)_{n-1}(HDO)_2^*$, those produced by the loss of $m - 1$ ($m = 1, 2, 3, \ldots, n$) molecules of H_2O from $H^+(H_2O)_n^*$ observed with the target gas, and those produced by unimolecular dissociation observed without the target gas, respectively. S_n^{n-m} indicates the ratio of clusters of a specific size that were produced by the unimolecular dissociation of $H^+(H_2O)_n$.

For the neutral mixed $(H_2O)_m(D_2O)_n$ cluster, the isotope effect has been experimentally observed and theoretically described using RRKM theory to have a large value of 30%,[20] whereas when the ion product distributions have been analyzed for the collision-induced dissociation of H_2O, HOD, or D_2O from $L^+(L_2O)_n$ (L = H, D; $n = 2-4$), the measured isotope effect has been found to be primarily disregarded (about 3%) in the protonated water cluster.[21] In addition, an ab initio calculation has suggested that $H^+(H_2O)_n$ can overcome negligibly small energy barriers among possible geometric isomers.[12] We therefore assumed that the vibrationally excited water cluster ions were freely interconverted to all of the geometric isomers and that H_2O, D_2O, and HDO molecules were released from the isomers with equal probability. Based on this assumption, the intensity I_n^{In} of the incorporation product was estimated[17] using the following equation from the intensities i_{n-m}^{Uex} and i_{n-m}^{Ex} of the observed daughter ions of $H^+(H_2O)_n(D_2O)^*$ and

$H^+(H_2O)_{n-1}(HDO)_2$*, respectively:

$$I_n^{In} = \sum_{m=1}^{n} \frac{{}_{n+1}C_m}{{}_nC_m}(i_{n-m}^{Uex} + i_{n-m}^{Ex}) \quad (5)$$

where ${}_nC_m$ represents the combination of numbers given as $n!/(n-m)!m!$. The intensity I_n^D of the dissociation product is given by

$$I_n^D = \sum_{m=1}^{n}\left(i_{n-m}^D - \frac{S_n^{n-m}}{S_n^n} i_n^P - \frac{{}_nC_{m-1}}{{}_nC_m}(i_{n-m}^{Uex} + i_{n-m}^{Ex})\right) \quad (6)$$

Branching fractions R_n^{In} for incorporation and R_n^D for dissociation are given by

$$R_n^{In} = \frac{I_n^{In}}{I_n^{In} + I_n^D} \quad (7)$$

and

$$R_n^D = \frac{I_n^D}{I_n^{In} + I_n^D} \quad (8)$$

respectively. The incorporation cross section, σ_n^{In}, and the dissociation cross section, σ_n^D, are given by

$$\sigma_n^{In} = R_n^{In}\sigma_n^r \quad (9)$$

and

$$\sigma_n^D = R_n^D\sigma_n^r \quad (10)$$

respectively.

3. Collision Energy Dependence of the Reaction Cross Section. Figure 3 shows the collision energy dependence of the reaction cross section in the collision of $H^+(H_2O)_n$ ($n = 4$ and 10) with D_2O. It can be seen from the figure that the total cross sections are strongly dependent on the collision energy. The total cross sections have the largest value of 202 ($n = 4$) and 734 Å^2 ($n = 10$) at 0.05 eV, which is the lowest collision energy used in this study, and decrease rapidly with an increase in the collision energy. In the region of the collision energy higher than approximately 0.40 ($n = 4$) and 0.80 eV ($n = 10$), the total cross sections decrease gradually with an increase in the collision energy and approach the geometrical cross sections of $H^+(H_2O)_n$ with D_2O.

The incorporation and dissociation cross sections in the collision of $H^+(H_2O)_n$ ($n = 4$ and 10) with D_2O are plotted as a function of the collision energy in Figure 3. We find that the incorporation and dissociation cross sections are strongly dependent on the collision energy. At high collision energy, the dissociation cross section is dominant, whereas at low collision energy, the incorporation cross section is dominant. As the collision energy decreases, the incorporation cross section dramatically increases. Similar collision-energy dependences of the reaction cross sections are observed for other sizes of protonated water clusters, $H^+(H_2O)_n$ ($n = 2-11$).

It has been reported[17] that the collision-energy dependence of the reaction probability for the incorporation of ND_3 into $H^+(NH_3)_n$ can be interpreted in terms of the transfer efficiency of the collision energy from the target gas to the internal energy of the parent cluster ion. This previous interpretation suggests

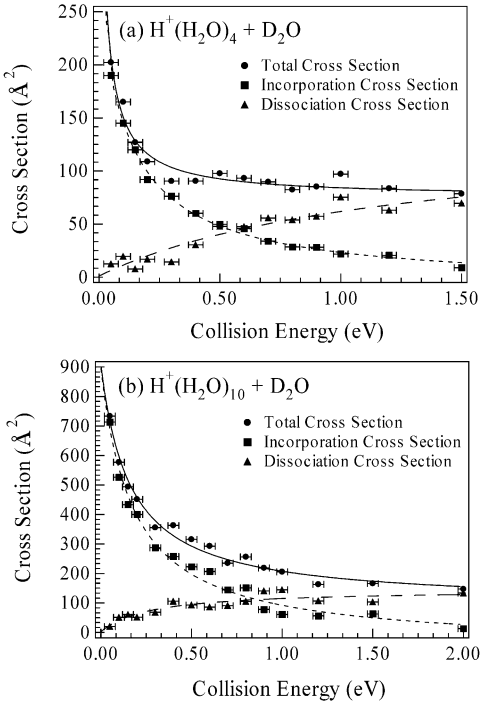

Figure 3. Collision energy dependence of total, incorporation, and dissociation cross sections of (a) $H^+(H_2O)_4 + D_2O$ and (b) $H^+(H_2O)_{10} + D_2O$.

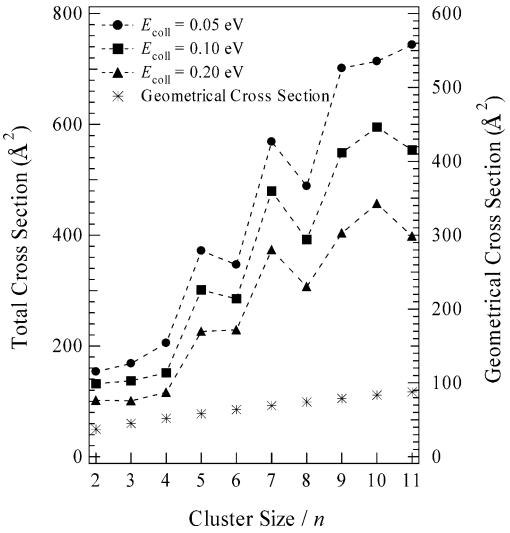

Figure 4. Cluster size dependence of the total cross section for $H^+(H_2O)_n$ ($n = 2-11$) at collision energies of 0.05, 0.10, and 0.20 eV, respectively. The asterisk (*) represents the geometrical cross section estimated from the density of liquid water.

that the D_2O molecule having a large impact parameter in the collision of $H^+(H_2O)_n$ ($n = 2-11$) with D_2O can be captured at low collision energy because the recoil energy decreases due to the small incident angle produced by the orbiting, and consequently, the reaction probability for incorporation increases in such a low-collision energy region. This interpretation suggests that incorporation is the dominant reaction at low collision energy.

4. Size Effect on the Total, Incorporation, and Dissociation Cross Sections. Figure 4 shows the total cross sections as a function of the size of the parent cluster ion. The cross sections increase drastically as the cluster size increases from $n = 4$ to 5, 6 to 7, and 8 to 9. For collision energies of 0.05 and 0.10 eV, the total cross sections have local minima at $n = 6$ and 8. At 0.20 eV, the total cross section at $n = 6$ slightly increases

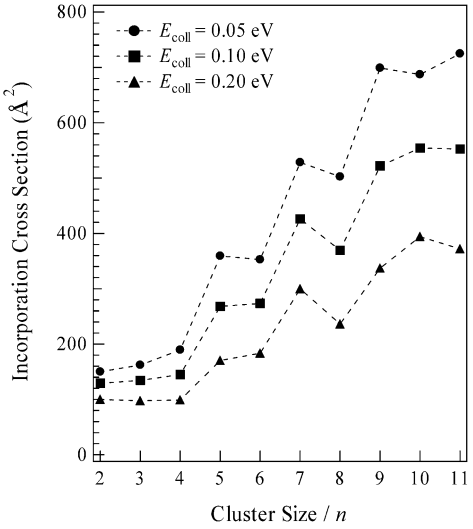

Figure 5. Cluster size dependence of the incorporation cross section for $H^+(H_2O)_n$ ($n = 2-11$) at collision energies of 0.05, 0.10, and 0.20 eV, respectively.

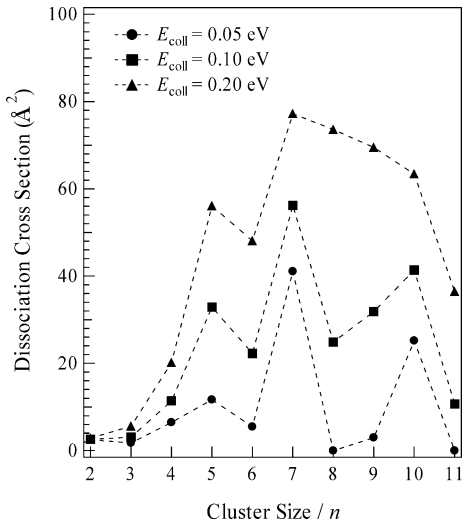

Figure 6. Cluster size dependence of the dissociation cross section for $H^+(H_2O)_n$ ($n = 2-11$) at collision energies of 0.05, 0.10, and 0.20 eV, respectively.

and at $n = 8$ has a local minimum. The geometrical cross sections of the water cluster ions, which are estimated from the density of liquid water, are plotted by the asterisk (*) in Figure 4. The geometrical cross section monotonically increases as the cluster size increases.

Figures 5 and 6 show the incorporation and dissociation cross sections, respectively, as a function of the size of the parent cluster ion. The incorporation cross section indicates a cluster-size dependence similar to that of the total cross section. The incorporation cross section increases drastically as the cluster size increases from $n = 4$ to 5, 6 to 7, and 8 to 9. For the collision energy of 0.05 eV, the incorporation cross section has local minima at $n = 6$ and 8. In addition, the dissociation cross section decreases as the cluster size increases from $n = 5$ to 6 and 7 to 8, as shown in Figure 6.

A cluster is stable when it has a particular "magic number" of constituent molecules. The magic number of the hydrogen-bonded ionic water cluster is associated with the thermodynamical stability due to its specific geometric structure.[22] The water molecule has an extremely high proton affinity and forms a very stable C_{3v} symmetric H_3O^+ hydronium ion with three equivalent protons, known as the Eigen cation.[4] In addition, the water

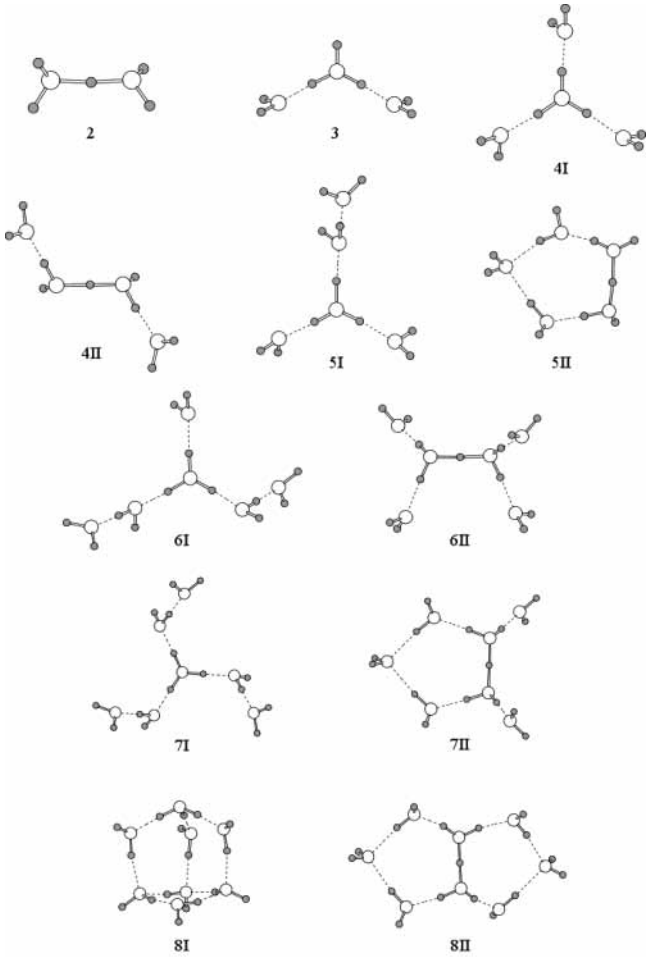

Figure 7. Ab initio optimized geometries of $H^+(H_2O)_n$ for $n = 2-8$. The O and H atoms are denoted by ○ and ●, respectively.

molecules form a C_2 symmetric $H_5O_2^+$ ion, sometimes called the Zundel cation, in which the proton is equally shared between two water molecules.[5] It has been reported that the respective cores of the Eigen and Zundel cations are completely surrounded by the first water shell at $n = 4$ and 6 and form symmetric $H_3O^+(H_2O)_3$ and $H_5O_2^+(H_2O)_4$, respectively.[22] First-principles Born−Oppenheimer molecular dynamics simulations suggest that the following new features are present for protonated water clusters of a size larger than $n = 7$, in which molecules tend to form two- and three-dimensional networks.[23] Basin-hopping Monte Carlo simulations indicate that water clusters $H^+(H_2O)_8$ have many low-energy structures, and that the most stable isomer has a symmetric cubic structure in which an H_3O^+ core ion and seven water molecules combine in three dimensions.[24] Therefore, the local minima of the cross sections at $n = 6$ and 8 shown in Figures 4−6 suggest that the water clusters $H^+(H_2O)_n$ have stable closed structures such as the symmetric $H_5O_2^+$-centered and cubic structures.

5. Collision Cross Section Calculated from the DFT-Based ab Initio Potential Curve. To obtain the collision cross section for the protonated water cluster $H^+(H_2O)_n$ ($n = 2-8$) with D_2O, density function theory (DFT) calculations were performed using the Gaussian 98 program package[25] with the cc-pVDZ basis set, where the hybrid density functional[26] was used in combination with the Lee, Yang, and Parr correlation functional (B3LYP)[27] to calculate the potential energy curves (PECs) for an attractive collision between $H^+(H_2O)_n$ and D_2O. For $H^+(H_2O)_n$ ($n = 2-8$), we selected the lowest-energy structures for each type of H_3O^+ or $H_5O_2^+$ ion core isomer in the total electronic

TABLE 1: Total Electronic Energy Change (ΔE) of the Clustering $H^+(H_2O) + (n-1)H_2O \rightarrow H^+(H_2O)_n$ ($n = 4-8$)

isomers $H^+(H_2O)_n$	ΔE (kcal/mol)
4 I	−88.9
4 II	−87.2
5 I	−105.0
5 II	−103.5
6 I	−119.7
6 II	−120.1
7 I	−133.0
7 II	−136.3
8 I	−156.4
8 II	−149.7

energy changes of the clustering $H^+(H_2O) + (n-1)H_2O \rightarrow H^+(H_2O)_n$, as shown in Figure 7. The optimized respective structures of $H^+(H_2O)_n$ and D_2O were fixed, and the distance between their centers of mass, R, was varied. The PECs between $H^+(H_2O)_n$ and D_2O, the orientation of which was optimized, were calculated for various Rs.

To calculate the collision cross sections, we used a classical molecular collision theory with the DFT-based ab initio PECs. When an impact parameter b is defined, the effective potential $V_{\text{eff}}(R)$ is given by

$$V_{\text{eff}}(R) = V(R) + \frac{E_{\text{coll}} b^2}{R^2} \tag{11}$$

where $V(R)$ is the potential for collision between $H^+(H_2O)_n$ and D_2O and E_{coll} is the collision energy. At a certain collision energy E_{coll}, the second term on the right-hand side of eq 11 behaves as a potential barrier with an increase in the impact parameter b. The maximum value of the impact parameter, b_{max}, at which the incident molecule having the collision energy E_{coll} can overcome the potential barrier gives the collision cross section. Therefore, the collision cross section, σ_n^{coll}, is given by

$$\sigma_n^{\text{coll}} = \pi b_{\text{max}}{}^2 \tag{12}$$

6. Comparison between the Total Cross Section and Collision Cross Section. Table 1 shows the total electronic energy changes (ΔE) of clustering for the H_3O^+ and $H_5O_2^+$ ion core structures shown in Figure 7 at $n = 4-8$. The structures of 6 II and 8 I are more stable than those of 6 I and 8 II by 0.4 and 6.7 kcal/mol, respectively. This result suggests that the $H^+(H_2O)_n$ at $n = 6$ and 8 are favored energetically to take the symmetric $H_5O_2^+$-centered structure 6 II and the cubic structure 8 I, respectively. We selected the most stable $H^+(H_2O)_n$ structures with the lowest ΔE among the clusters illustrated in Figure 7 and calculated the collision cross sections for their most stable structures. Figure 8 shows the collision cross section of $H^+(H_2O)_n$ calculated as a function of the cluster size $n = 2-8$. At the collision energy of 0.05 eV, our calculations show that the collision cross section has local minima at $n = 6$ and 8, at which the structures of 6 II and 8 I are selected as the most stable structures, respectively. At collision energies of 0.10 and 0.20 eV, the collision cross section slightly increases at $n = 6$ and has a local minimum at $n = 8$. These results are consistent with the tendency of the total cross section obtained from the experiment for $n = 6$ and 8. Only the selected structures of 4I, 5I, 6II, 7II, and 8I can reproduce the experimental curve showing local minima at $n = 6$ and 8. This finding therefore suggests that these selected structures are most probable for the $H^+(H_2O)_n$ clusters generated in our experiments. In addition, we conclude that the local minima of the total cross section at $n = 6$ and 8, shown in Figure 4, are related to the small values of the collision cross section for $H^+(H_2O)_6$ and for $H^+(H_2O)_8$ with the closed structures of symmetric $H_5O_2^+$-centered structure 6 II and cubic structure 8 I, respectively. Such closed structures with the small geometrical cross sections cause a decrease in the attractive force between the solvent molecule in the cluster ion and a D_2O molecule and thereby result in small collision cross sections and small total cross sections. In contrast, at $n = 5$ and 7, water cluster ions have the structures 5 I and 7 II, respectively, in which the water molecule present on the outermost shell causes a large geometrical cross section and a large collision cross section.

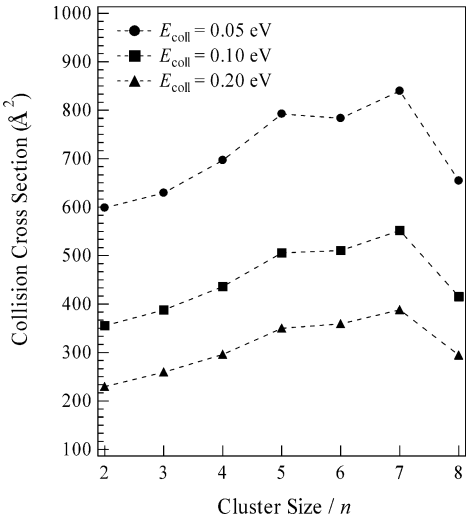

Figure 8. Cluster size dependence of the collision cross section for $H^+(H_2O)_n$ ($n = 2-8$) at collision energies of 0.05, 0.10, and 0.20 eV, respectively.

Conclusions

We investigated the collisions of size- and translational-energy-selected protonated water clusters $H^+(H_2O)_n$ ($n = 2-11$) under a single-collision condition with D_2O using guided-ion beam tandem mass spectrometry. Two types of reactions, incorporation and dissociation, were observed in the collisions, and these reaction cross sections were determined as a function of the collision energy. Our results demonstrated that the incorporation cross section is dominant at low collision energy and that the dissociation cross section is increased as the collision energy increases. The total cross section was found to depend strongly on the cluster size; the cross section drastically increased as the cluster size increased from $n = 4$ to 5, 6 to 7, and 8 to 9 and had local minima at $n = 6$ and 8 at respective collision energies of 0.05 and 0.10 eV. The collision cross section calculated from the DFT-based ab initio potential curve had a tendency similar to the cluster size dependence of the total cross section. From a comparison of the collision cross section with the total cross section, we found that the local minima of the total cross section at $n = 6$ and 8, respectively, originated from the symmetric $H_5O_2^+$-centered structure for $H^+(H_2O)_6$ and the cubic structure for $H^+(H_2O)_8$, which are the most stable energetically.

References and Notes

(1) Viggiano, A. A. *Mass Spectrom. Rev.* **1993**, *12*, 115.

(2) Turco, R. P.; Zhao, J.-X.; Yu, F. *Geophys. Res. Lett.* **1998**, *25*, 635.

(3) Mactaylor, R. S.; Castleman, A. W., Jr. *J. Atmos. Chem.* **2000**, *36*, 23.

(4) Eigen, M. *Ang. Chem., Int. Ed. Eng.* **1964**, *3*, 1.

(5) Zundel, G. In *The Hydrogen Bond-Recent Developments in Theory and Experiment*; Schuster, P., Zundel, G., Sandorfy, C., Eds.; North-Holland: Amsterdam, 1976; Vol. 2, Chapter 15.
(6) Downing, H. D.; Williams, D. *J. Phys. Chem.* **1976**, *80*, 1640.
(7) Giguère, P. A. *J. Chem. Educ.* **1979**, *56*, 571.
(8) Giguère, P. A. *Chem. Phys.* **1981**, *60*, 421.
(9) Librovich, N. B.; Sakun, V. P.; Sokolov, N. D. *Chem. Phys.* **1981**, *60*, 425.
(10) Agmon, N. *J. Phys. Chem.* **1998**, *102*, 192.
(11) Kameda, Y.; Usuki, T.; Uemura, O. *Bull. Chem. Soc. Jpn.* **1998**, *71*, 1305.
(12) Jiang, J.-C.; Wang, Y.-S.; Chang, H.-C.; Lin, S. H.; Lee, Y. T.; Niedner-Schatteburg, G.; Chang, H.-C. *J. Am. Chem. Soc.* **2000**, *122*, 1398.
(13) Honma, K.; Sunderlin, L. S.; Armentrout, P. B. *Int. J. Mass Spectrom. Ion Processes* **1992**, *117*, 237.
(14) Honma, K.; Sunderlin, L. S.; Armentrout, P. B. *J. Chem. Phys.* **1993**, *99*, 1623.
(15) Schindler, T.; Berg, C.; Niedner-Schatteburg, G.; Bondybey, V. E. *J. Chem. Phys.* **1996**, *104*, 3998.
(16) Smith, D.; Adams, N. G.; Henchman, M. J. *J. Chem. Phys.* **1980**, *72*, 4951.
(17) Orii, T.; Okada, Y.; Takeuchi, K.; Ichihashi, M.; Kondow, T. *J. Chem. Phys.* **2000**, *113*, 8026.
(18) Yamaguchi, S.; Kudoh, S.; Okada, Y.; Orii, T.; Takeuchi, K. *Chem. Phys. Lett.* **2002**, *359*, 480.
(19) Ichihashi, M.; Nonose, S.; Nagata, T.; Kondow, T. *J. Chem. Phys.* **1994**, *100*, 6458.
(20) Kay, B. D.; Castleman, A. W., Jr. *J. Chem. Phys.* **1983**, *78*, 4297.
(21) Graul, S. T.; Brickhouse, M. D.; Squires, R. R. *J. Am. Chem. Soc.* **1990**, *112*, 631.
(22) Niedner-Schatteburg, G.; Bondybey, V. E. *Chem. Rev.* **2000**, *100*, 4059.
(23) Cheng, H.-P. *J. Phys. Chem.* **1998**, *102*, 6201.
(24) Singer, S. J.; McDonald, S.; Ojamäe, L. *J. Chem. Phys.* **2000**, *112*, 710.
(25) Frisch, M. J.; Trucks, G. W.; Schlegel, H. B.; Scuseria, G. E.; Robb, M. A.; Cheeseman, J. R.; Zakrzewski, V. G.; Montgomery, J. A., Jr.; Stratmann, R. E.; Burant, J. C.; Dapprich, S.; Millam, J. M.; Daniels, A. D.; Kudin, K. N.; Strain, M. C.; Farkas, O.; Tomasi, J.; Barone, V.; Cossi, M.; Cammi, R.; Mennucci, B.; Pomelli, C.; Adamo, C.; Clifford, S.; Ochterski, J.; Petersson, G. A.; Ayala, P. Y.; Cui, Q.; Morokuma, K.; Malick, D. K.; Rabuck, A. D.; Raghavachari, K.; Foresman, J. B.; Cioslowski, J.; Ortiz, J. V.; Stefanov, B. B.; Liu, G.; Liashenko, A.; Piskorz, P.; Komaromi, I.; Gomperts, R.; Martin, R. L.; Fox, D. J.; Keith, T.; Al-Laham, M. A.; Peng, C. Y.; Nanayakkara, A.; Gonzalez, C.; Challacombe, M.; Gill, P. M. W.; Johnson, B. G.; Chen, W.; Wong, M. W.; Andres, J. L.; Head-Gordon, M.; Replogle, E. S.; Pople, J. A. *Gaussian 98*, revision A.7; Gaussian, Inc.: Pittsburgh, PA, 1998.
(26) Beck, A. D. *J. Chem. Phys.* **1993**, *98*, 5648.
(27) Lee, C.; Yang, W.; Parr, R. G. *Phys. Rev.* **1988**, *37B*, 785.